PAPER

Crown-ether coordination compounds of zirconium, hafnium and scandium using metal nanoparticles†

Lara-Pauline Faden,[a] Lkhamsuren Bayarjargal, [iD] [b] Victor Milman, [iD] [c] Björn Winkler [iD] [b] and Claus Feldmann [iD] *[a]

Crown-ether coordination compounds of zirconium, hafnium and scandium were rarely reported in the past. Conventional syntheses *via* Lewis-acid–base reactions or metathesis reactions suffer from the high Lewis acidity and high oxophilicity of Zr^{4+}, Hf^{4+} and Sc^{3+}. Therefore, a redox approach using nanoparticles of zerovalent zirconium, hafnium, and scandium is suggested here. Zr(0), Hf(0), Sc(0) nanoparticles, 2–8 nm in size, are prepared by reduction of $ZrCl_4$, $HfCl_4$ and $ScCl_3$ with sodium naphthalenide in a liquid-phase synthesis. The as-prepared Zr(0), Hf(0), Sc(0) nanoparticles are reacted in ionic liquids with 12-crown-4 (12c4), 15-crown-5 (15c5) and 18-crown-6 (18c6) exhibiting ring-opening diameters of 140 to 300 pm. As a result, four new crown-ether coordination complexes are obtained and characterized by single-crystal structure X-ray analysis. The structural variety ranges from the layered structure $[AlCl_2(12c4)][NaAl_2Cl_8]$ (**1**) over the chiral chain-type compounds $[ZrCl_2(15c5)][Na_2Al_4Cl_{16}]$ (**2**) and $[HfCl_2(15c5)][Na_2Al_4Cl_{16}]$ (**3**) to $[ScCl_2(18c6)][AlCl_4]$ (**4**) with isolated ions. All compounds crystallize in space groups without inversion symmetry. Exemplarily, this was confirmed *via* second-harmonic generation (SHG) measurements of $[ZrCl_2(15c5)][Na_2Al_4Cl_{16}]$ and $[ScCl_2(18c6)][AlCl_4]$, whereof the latter shows a strong SHG signal (comparable to KH_2PO_4/KDP) and appears to be phase matchable.

1. Introduction

The knowledge of crown-ether coordination compounds of zirconium, hafnium and scandium is rather limited. Although crown ethers are known as versatile chelating ligands, which can coordinate almost all types of cations,[1] compounds containing zirconium/hafnium/scandium and a crown ether usually show the crown ether coordinated to other metal cations or even non-coordinated in the crystal structure. Examples are $[(H_2DA18\text{-crown-}6)(M_2F_{10}\cdot 2H_2O)\cdot 2H_2O]$ (M: Zr, Hf), $[Sc(NO_3)_3(H_2O)_3](18\text{-crown-}6)$, $[Sc(H_2O)_4]_2[calix[4]arene (SO_3)_4\text{-H}]_2(18\text{-crown-}6)\cdot 16H_2O$, or $[Sc(H_2O)_4(NCS)_2]$ $[Sc(H_2O)_2 (NCS)_4]\cdot 2(18\text{-crown-}6)$.[2] Specifically, a coordination of Zr^{4+} and Hf^{4+} by a crown ether was observed for a few compounds only,

including $[ZrCl_2(12\text{-crown-}4)]$ or $[(Bn_2Cyclam)ZrCl_2]$.[3] It was even reported that the crown ether was split into chain-like fragments in the presence of Zr^{4+} and Hf^{4+}, which can be ascribed to their high Lewis-acidity.[4] In contrast to Zr^{4+} and Hf^{4+}, coordination of Sc^{3+} with crown ethers was reported more often (*e.g.*, $[ScCl(dibenzo\text{-}18\text{-crown-}6)(MeCN)][SbCl_6]_2$, $[ScCl_2(12\text{-crown-}4)][SbCl_6]$, or $[ScCl_2(18\text{-crown-}6)][FeCl_4]$).[5]

Due to the high Lewis acidity of Zr^{4+}, Hf^{4+}, Sc^{3+} as well as their highly oxophilic character,[6] syntheses in conventional solvents such as water, ethanol, THF, *etc*., promote the formation of oxocomplexes and a coordination with solvent molecules.[2–5] As an alternative to the most often used Lewis-acid–base reactions or metathesis reactions,[2–5] a redox approach could be an alternative option for the synthesis of crown-ether coordination compounds. The bulk metals zirconium, hafnium, scandium, however, show only low reactivity due to low solubility, low surface area and passivation by metal–oxide layers.[7] In contrast, nanoparticles of these metals can be expected to be much more reactive, especially in the liquid phase and at moderate temperatures. Aiming at Zr(0), Hf(0) and Sc(0) metal nanoparticles, the number of publications has been limited until now. Zerovalent metal nanoparticles have been only accessible *via* physical methods such as evaporation techniques, laser ablation, sonochemical

[a]*Institute for Inorganic Chemistry, Karlsruhe Institute of Technology (KIT), Engesserstrasse 15, D-76131 Karlsruhe, Germany. E-mail: claus.feldmann@kit.edu*
[b]*Institute of Geosciences, Goethe University Frankfurt, Altenhoeferallee 1, D-60438 Frankfurt a. M., Germany*
[c]*Dassault Systèmes BIOVIA, Cambridge, UK*

methods or solid-state reactions,[8] resulting in large particles (>50 nm) with certain agglomeration, broad size distributions and/or significant oxygen contamination. A liquid-phase synthesis of nanoparticles of these metals was shown by us only recently for the first time.[9]

In the following, we use Zr(0), Hf(0), Sc(0) nanoparticles with a size of 2–8 nm as reactive starting material to perform reactions with the crown ethers 12-crown-4, 15-crown-5 and 18-crown-6 in ionic liquids. As a result, the novel crown-ether coordination compounds $[AlCl_2(12c4)][NaAl_2Cl_8]$ (**1**), $[ZrCl_2(15c5)][Na_2Al_4Cl_{16}]$ (**2**) and $[HfCl_2(15c5)][Na_2Al_4Cl_{16}]$ (**3**) as well as $[ScCl_2(18c6)][AlCl_4]$ (**4**) were obtained. Beside the novel crown-ether coordination of Zr^{4+}/Hf^{4+}, interesting chain-type and layer-type anions as well as second harmonic generation (SHG) effects were observed.

2.   Experimental section

2.1   General

All reactions and sample handling were carried out under dried argon atmosphere using standard Schlenk techniques or argon-filled glove boxes (MBraun Unilab, $c(O_2, H_2O) < 0.1$ ppm). This also included all centrifugation and washing procedures. Moreover, all sample transfers for analytical characterization were performed under strict inert conditions (*e.g.* by using suitable transfer modules). Reactions were performed in Schlenk flasks and glass ampoules that were evacuated ($p < 10^{-3}$ mbar), heated, and flushed with argon three times prior to use. The starting materials $ScCl_3$ (99.99%, ABCR), $ZrCl_4$ (99.9%, ABCR), $HfCl_4$ (99.9%, ABCR), naphthalene (99%, Alfa Aesar), sodium (99%, Sigma-Aldrich), 12-crown-4 (98%, ABCR), 15-crown-5 (98%, ABCR), 18-crown-6 (99%, Alfa Aesar), and $AlCl_3$ (99.99%, Sigma-Aldrich) were used as received.

Tetrahydrofuran (THF, 99%, Seulberger) was refluxed for three days and freshly destilled over sodium. 1-Butyl-3-methyl-imidazoliumchloride ([BMIm]Cl, 99%, IOLiTec) was dried under reduced pressure (10^{-3} mbar) at 130 °C for 72 h. Since [BMIm]Cl (melting point: +70 °C) is solid at and above room temperature, $AlCl_3$ was added to form $[BMIm][AlCl_4]$ as ionic liquid. By increasing the amount of $AlCl_3$ (relative to the concentration of [BMIm]Cl), moreover, the Lewis acidity of the ionic liquid was increased, which often accelerates reaction and crystallisation.

2.2   Synthesis of metal nanoparticles

Zr(0) nanoparticles. 117 mg of $ZrCl_4$ (0.5 mmol) were dissolved in 10 ml of THF. Moreover, 46 mg of sodium (2.0 mmol) and 260 mg of naphthalene (2.0 mmol) were dissolved in 5 mL of THF at room temperature to obtain a deep green solution of sodium naphthalenide ([NaNaph]). Dissolution requires certain time and heating to obtain THF-coordinated $ZrCl_4$ After complete dissolution of the starting materials, the [NaNaph] solution was injected into the $ZrCl_4$ solution at room temperature with vigorous stirring. It needs

to be noticed that stirring must be performed with glass stirring rods to avoid any reaction of the reactive metals with the Teflon coating of standard stirring rods. After the reaction, the Zr(0) nanoparticles were separated by centrifugation (25 000 rpm, 55 200*g*). They were purified by resuspension/centrifugation in/from THF. Finally, the Zr(0) nanoparticles were dried in vacuum at room temperature. Powder samples were obtained with a yield of 90–95%. The loss was predominately due to centrifugation with some Zr(0) nanoparticles remaining adsorbed to the surface of the centrifugation tubes.

Hf(0) nanoparticles. These nanoparticles were prepared similar to the aforementioned Zr(0) nanoparticles. Specifically, 160 mg of $HfCl_4$ (0.50 mmol), 46.0 mg of sodium (2.0 mmol) and 260 mg of naphthalene (2.0 mmol) were used.

Sc(0) nanoparticles. 76 mg of $ScCl_3$ (0.5 mmol), 34.5 mg of sodium (1.5 mmol) and 195 mg of naphthalene (1.5 mmol) were stirred in 15 mL THF over a period of 12 hours at room temperature. It needs to be noticed that stirring must be performed with glass stirring rods to avoid any reaction of the reactive metals with the Teflon coating of standard stirring rods. After the reaction, the Sc(0) nanoparticles were separated by centrifugation (25 000 rpm, 55 200*g*). They were purified by resuspension/centrifugation in/from THF. Finally, the metal nanoparticles were dried in a vacuum at room temperature. Powder samples were obtained with a yield of 90–95%. The loss was predominately due to centrifugation with some Sc(0) nanoparticles remaining adsorbed to the surface of the centrifugation tubes.

2.3   Crown-ether coordination compounds

$[AlCl_2(12c4)][NaAl_2Cl_8]$ **(1)**. 150.0 mg of [BMIm]Cl (0.86 mmol), 343.5 mg of $AlCl_3$ (2.58 mmol), 41.0 mg of dried Zr(0) nanoparticles (0.45 mmol), 46.6 mg of $ZrCl_4$ (0.20 mmol) and 0.05 mL of 12-crown-4 were heated under argon in a sealed glass ampoule for 96 h at 120 °C. After cooling to room temperature with a rate of 1 K h^{-1}, the **1** was obtained as colourless crystals with quantitative yield. The title compound is highly sensitive to moisture.

Here it should be noticed that compound **1** can be also prepared in absence of $ZrCl_4$. As our examination aimed at the coordinative situation of different crown ethers with Zr^{4+}, we liked to include the information that a coordination of Al^{3+} by 12c4 was preferred over a coordination of Zr^{4+} with the here applied conditions.

$[ZrCl_2(15c5)][Na_2Al_4Cl_{16}]$ **(2)**. 150.0 mg of [BMIm]Cl (0.86 mmol), 343.5 mg of $AlCl_3$ (2.58 mmol), 41.0 mg of dried Zr(0) nanoparticles (0.45 mmol) and 53.0 mg of 18-crown-6 (0.20 mmol) were heated under argon in a sealed glass ampoule for 96 h at 120 °C. After cooling to room temperature with a rate of 1 K h^{-1}, the title compound was obtained as colourless crystals with quantitative yield. The title compound is highly sensitive to moisture.

$[HfCl_2(15c5)][Na_2Al_4Cl_{16}]$ **(3)**. 150.0 mg of [BMIm]Cl (0.86 mmol), 343.5 mg of $AlCl_3$ (2.58 mmol), 57.1 mg of dried Hf(0) nanoparticles (0.32 mmol) and 53.0 mg of 18-crown-6 (0.20 mmol) were heated under argon in a sealed glass

ampoule for 96 h at 120 °C. After cooling to room temperature with a rate of 1 K h^{-1}, the title compound was obtained as colourless crystals with quantitative yield. The title compound is highly sensitive to moisture.

[ScCl$_2$(18c6)][AlCl$_4$] (4). 200.0 mg of [BMIm]Cl (1.14 mmol), 152.7 mg of AlCl$_3$ (1.14 mmol), 22.5 mg of dried Sc(0) nanoparticles (0.50 mmol) and 66.0 mg of 18-crown-6 (0.25 mmol) were heated under argon in a sealed glass ampoule for 96 h at 120 °C. After cooling to room temperature with a rate of 1 K h^{-1}, the **4** was obtained as colourless crystals with quantitative yield. The title compound is highly sensitive to moisture.

2.3   Analytical methods

Detailed information on the applied analytical methods can be found in the ESI.†

3.   Results and discussion

3.1   Zirconium, hafnium, scandium metal nanoparticles

The synthesis of Zr(0), Hf(0) and Sc(0) nanoparticles follows our previously reported approach to obtain reactive base-metal nanoparticles in the liquid phase.[9] ZrCl$_4$, HfCl$_4$ and ScCl$_3$ were used as most common starting materials. In the case of Zr(0) and Hf(0), ZrCl$_4$ and HfCl$_4$ can be dissolved in THF with formation of THF complexes. Afterwards, a solution of sodium naphthalenide ([NaNaph]) in THF was injected into the ZrCl$_4$/HfCl$_4$ solution with vigorous stirring. The formation of Zr(0)/Hf/(0) nanoparticles is indicated by the instantaneous formation of deep-black suspensions (Fig. 1).[9a] The synthesis of Sc(0) nanoparticles follows the synthesis of the Zr(0)/Hf(0) nanoparticles, in principle. Due to the insufficient solubility of ScCl$_3$, however, sodium, naphthalene, and ScCl$_3$ were simultaneously added to THF. After 12 hours of intense stirring, the reduction and nucleation of the Sc(0) nanoparticles were completed and also resulted in a deep-black suspension (Fig. 1). This one-pot approach used to obtain Sc(0) nanoparticles

seems disadvantageous for the nucleation of small-sized nanoparticles at first sight. The chemical equilibria with a very slow dissolution of ScCl$_3$ and a very fast reduction of Sc^{3+} to Sc(0) as well as the low solubility of the zerovalent metal in THF, however, promote the nucleation of small particles.[10]

For purification, the as-prepared Zr(0)/Hf(0)/Sc(0) nanoparticles were centrifugated/redispersed in/from THF to remove remaining naphthalene. NaCl is almost insoluble in THF and cannot be removed. A dissolution and removal of NaCl would require a more polar solvent such as methanol, which, however, would oxidize the metal nanoparticles. Finally, the Zr(0)/Hf(0)/Sc(0) metal nanoparticles were dried at room temperature in vacuum to obtain powder samples.

Particle size and particle size distribution of the as-prepared Zr(0), Hf(0) and Sc(0) nanoparticles were examined by transmission electron microscopy (TEM). TEM images show spherical particles with uniform size and low degree of agglomeration (Fig. 2). A statistical evaluation of >200 nanoparticles on TEM images reveals mean sizes of 2–8 nm (Table 1). High-resolution (HR)TEM images confirm the size of the nanoparticles and evidence the monocrystallinity of the as-prepared Zr(0), Hf(0), Sc(0) nanoparticles with lattice fringes extending through the whole particle (Fig. 2). The lattice plane distances are in good agreement with those of the respective bulk metals (Table 1). This finding is also confirmed by Fourier-transform (FT) analysis, which is in accordance with the calculated diffraction pattern of hexagonal bulk-Zr(0) ($P6_3/mmc$, $a = 3.233$, $c = 5.147$ Å) in the [001] zone axis,[11] a slightly distorted hexagonal closed packed structure of bulk-Hf(0) ($P6_3/mmc$, $a = 3.198$, $c = 5.061$ Å, $\gamma = 115° \pm 3°$) in the [001] zone axis,[12] and hexagonal bulk-Sc(0) ($P6_3/mmc$, $a = 3.296$, $c = 5.275$ Å) in the [211] zone axis.[13] The intensity of the Bragg reflections is low due to the small size of the base-metal nanoparticles.

The as-prepared Zr(0), Hf(0), and Sc(0) nanoparticles are highly sensitive to moisture, air and other oxidizing agents. Therefore, all reactions and sample handling need to be per-
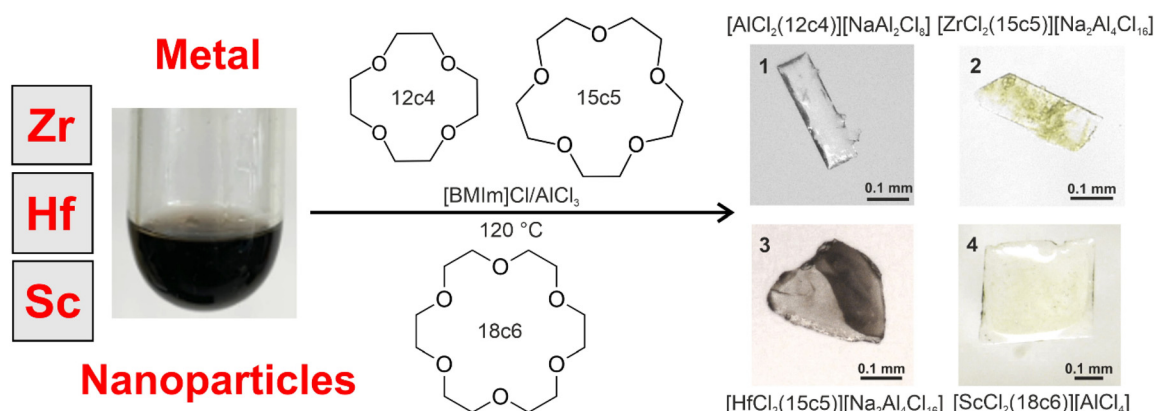

Fig. 1   Scheme illustrating the synthesis of Zr(0), Hf(0), Sc(0) nanoparticles (with photos of the respective suspensions and powder samples) as well as their reaction with the crown ethers 12-crown-4, 15-crown-5 and 18-crown-6 in [BMIm]Cl/AlCl$_3$ as the ionic liquid (with photos of single crystals of the compounds **1–4**).
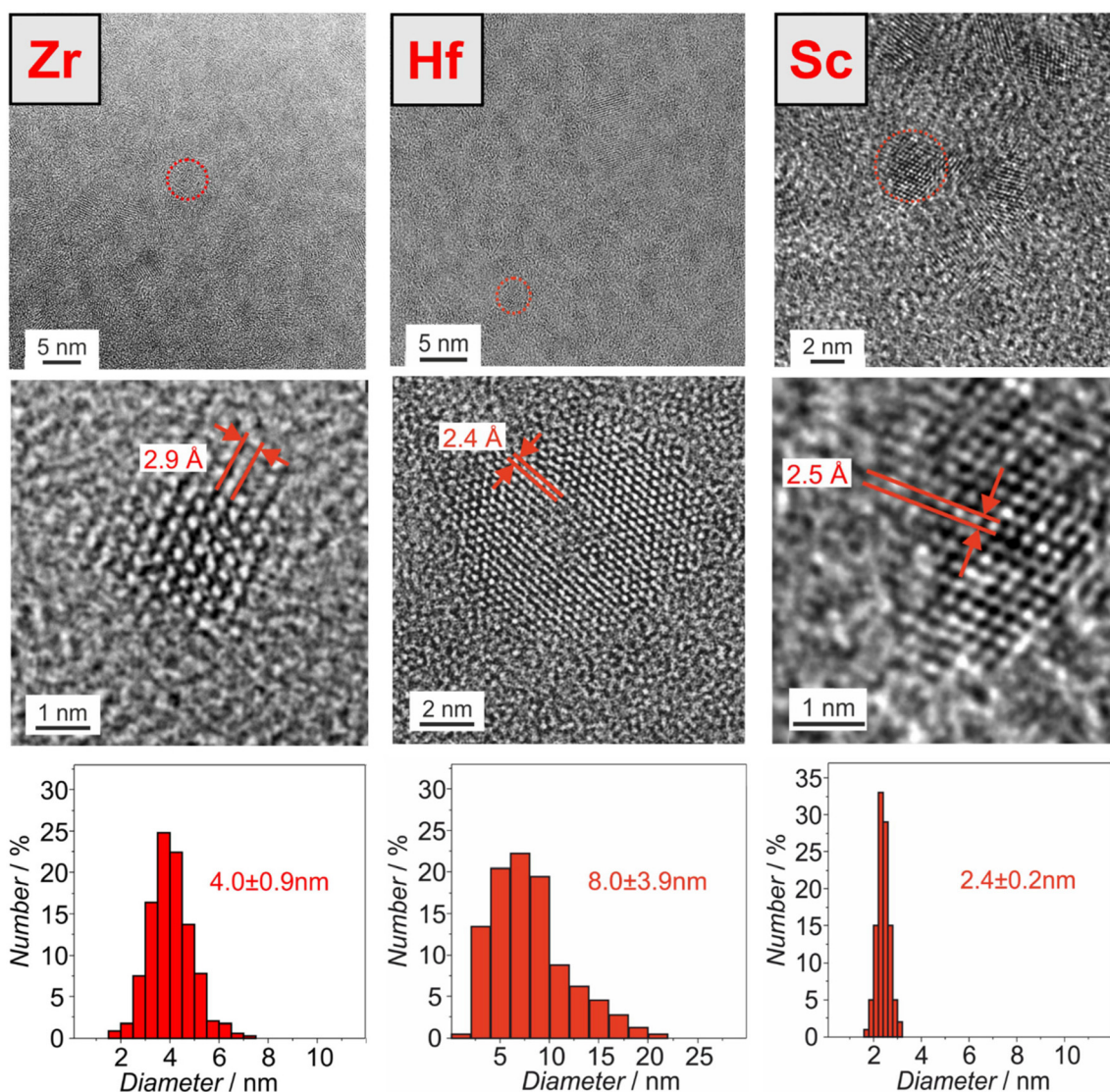
Fig. 2 TEM images of the as-prepared Zr(0), Hf(0), Sc(0) nanoparticles with overview images (top), HRTEM images of single nanoparticles (middle), and size distribution (bottom; obtained by statistical evaluation of >100 nanoparticles on TEM images).

Table 1 Mean size and lattice plane distances of Zr(0), Hf(0) and Sc(0) nanoparticles

Metal	Mean size/nm	Measured lattice plane distance/Å	Lattice plane distance of bulk reference/Å
Zr(0)	4.0 ± 0.9	2.9	Hexagonal β-Zr(0): d_{100} with 2.8 Å (ref. 11)
Hf(0)	8.0 ± 3.9	2.6	Hexagonal Hf(0): $d_{\bar{1}10}$ with 2.7 Å (ref. 12)
Sc(0)	2.4 ± 0.2	2.5	Hexagonal Sc(0): $d_{0\bar{1}1}$ with 2.5 Å (ref. 13)

formed with inert conditions (dried argon or nitrogen, vacuum), using standard Schlenk techniques or glove boxes. This also includes centrifugation and all analytical characterization. Attention must be paid to avoid contact of the Zr(0), Hf(0) and Sc(0) nanoparticles with water, air or other oxidizing agents, which can lead to violent combustion or explosion. Generally, the reactivity of the metal nanoparticles can be considered to be comparable to those of the heavy alkali metals rubidium and cesium.

3.2 Crown-ether coordination compounds

Reactions of the Zr(0), Hf(0), and Sc(0) nanoparticles were performed with the crown ethers 12-crown-4 (12c4), 15-crown-5 (15c5), and 18-crown-6 (18c6), exhibiting different ring-opening sizes of about 140, 180, and 300 pm.[1,14] In order to exclude solvent molecules to act as ligands in the products, all reactions were performed in [BMIm]Cl/AlCl$_3$ as ionic liquid (BMIm: 1-butyl-3-methylimidazolium; see ESI†). Ionic liquids

as solvents seemed promising due to their weakly-coordinating properties as well as due to their chemical and thermal stability.[15] As a result, the compounds $[AlCl_2(12c4)][NaAl_2Cl_8]$ (**1**), $[ZrCl_2(15c5)][Na_2Al_4Cl_{16}]$ (**2**), $[HfCl_2(15c5)][Na_2Al_4Cl_{16}]$ (**3**) and $[ScCl_2(18c6)][AlCl_4]$ (**4**) were obtained with quantitative yield after four days at 120 °C. The colourless crystals of the title compounds are sensitive to moisture and need to be handled and stored under inert conditions.

As a first reaction, the smallest crown ether 12c4 was reacted with Zr(0) nanoparticles in [BMIm]Cl/AlCl$_3$. 12c4 is well-known for selective coordination of Li$^+$ cations,[16] which exhibit a similar cation size as Zr^{4+} (r(Li$^+$) = 0.73 Å; r(Zr^{4+}) = 0.73 Å).[17] In contrast to our expectation, however, the obtained colourless crystals were identified as $[AlCl_2(12c4)][NaAl_2Cl_8]$ (**1**), which contains 12c4 coordinated to Al^{3+} instead of Zr^{4+}. The formation of **1** can be ascribed to the following reaction with NaCl originating from the reduction of ZrCl$_4$ with [NaNaph]:

$$12c4 + (ZrCl_4) + NaCl + 3AlCl_3 \rightarrow [AlCl_2(12c4)][NaAl_2Cl_8] + (ZrCl_4)$$
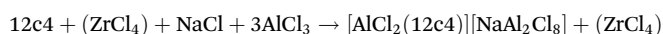
Although present in the reaction, a coordination of Al^{3+} by 12c4 was obviously preferred over a coordination of Zr^{4+}. Despite of the absence of zirconium, **1** nevertheless shows interesting structural features. Thus, the compound crystallizes in the non-centrosymmetric space group $P2_12_12_1$ (ESI: Table S1 and Fig. S1†) and consists of $[AlCl_2(12c4)]^+$ cations and layered $^2_\infty[NaAl_2Cl_8]^-$ anions (Fig. 3). The $[AlCl_2(12c4)]^+$ cation shows Al^{3+} with a distorted octahedral coordination with a κ^4-12c4 ligand as well as two Cl$^-$ (Al–O: 190.3(15)–202.2 (12) pm; Al–Cl: 219.0(7)–219.5(7) pm) (Fig. 3a), which is comparable to $[AlCl_2(12c4)][AlCl_3Et]$ (Al–O: 192(1)–199(1) pm; Al–Cl: 220.0(8)–220.2(5) pm).[18] The corrugated, layered $^2_\infty[NaAl_2Cl_8]^-$ anion extends along the crystallographic a,b plane and consists of distorted trigonal NaCl$_6$ prisms (Na–Cl: 278.7(9)–310.1(11) pm) and distorted AlCl$_4$ tetrahedra (Al–Cl: 209.8(7)–216.7(7) pm; Cl–Al–Cl: 106.1(3)–113.1(3)°) (Fig. 3b). The NaCl$_{6/2}$ prisms are interlinked via all Cl atoms to four AlCl$_4$ tetrahedra, while all AlCl$_4$ tetrahedra are connected to two NaCl$_6$ prisms. The two crystallographically different AlCl$_4$ tetrahedra include a Al(2)Cl$_{2/1}$Cl$_{2/2}$ connectivity with two corner-bridging Cl and two terminal Cl along the a axis as well

as a Al(3)Cl$_{4/2}$ connectivity with edge-bridging of all Cl atoms to two NaCl$_6$ prisms along the b axis (Fig. 3b).

As the reaction of Zr(0) nanoparticles with 12c4 did not result in a coordination with Zr^{4+}, the synthesis was repeated with the larger crown ether 15c5. This results in colourless, transparent crystals of $[ZrCl_2(15c5)][Na_2Al_4Cl_{16}]$ (**2**), which crystallize in the non-inversion symmetric space group $P2_1$ (ESI: Table S2 and Fig. S2†). **2** consists of a chain of $[ZrCl_2(15c5)]^{2+}$ cations and $^1_\infty[Na_2Al_4Cl_{16}]^{2-}$ anions (Fig. 4). Analogously, the reaction can be performed with Hf(0) nanoparticles, resulting in $[HfCl_2(15c5)][Na_2Al_4Cl_{16}]$ (**3**) with a similar composition (ESI: Table S3 and Fig. S3†). The formation of **2** and **3** can be rationalized based on an oxidation of zirconium with a reduction of aluminum of the ionic liquid:

$$3M + 315c5 + 6NaCl + 16AlCl_3$$
$$\rightarrow 3[MCl_2(15c5)][Na_2Al_4Cl_{16}] + 4Al \quad (M = Zr, Hf)$$
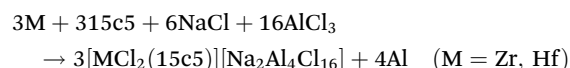
The $[ZrCl_2(15c5)]^{2+}$ cation contains Zr^{4+} with nearly planar κ^5-coordinated 15c5 (Zr–O: 213.2(7)–216.4(8) pm) and two axial Cl$^-$ (Zr–Cl: 237.5(3)–240.9(3) pm), in sum, resulting in a distorted pentagonal bipyramidal arrangement (O–Zr–O: 71.3(3)–73.4(3)°; Cl–Zr–Cl: 176.8(1)°) (Fig. 4a). It should also be noticed that one of the axial Cl$^-$ of the $[ZrCl_2(15c5)]^{2+}$ cation also shows a short distance to Na$^+$ in the $^1_\infty[Na_2Al_4Cl_{16}]^{2-}$ chain, forming a capped trigonal NaCl$_7$ prism (Na–Cl: 321.4(6) pm). The anionic $^1_\infty[Na_2Al_4Cl_{16}]^{2-}$ chains are oriented along the a axis and consist of distorted, trigonal NaCl$_6$ prisms and distorted AlCl$_4$ tetrahedra (Fig. 4b). Sodium exhibits two different crystallographic sites with Na(1) (Na–Cl: 280.1(5)–299.8(6) pm) and Na(2) (Na–Cl: 275.7(5)–321.4(6) pm), whereof Na(2) shows the aforementioned additional coordination to one of the chlorine atoms of the cation (Na–Cl: 321.4(6) pm), in sum resulting in a capped, trigonal NaCl$_7$ prism (Fig. 4b). The AlCl$_4$ tetrahedra (Al–Cl: 210.1(4)–215.7(4) pm) show corner-sharing with one NaCl$_6$ unit and edge-sharing with a second NaCl$_6$ unit. This results in an AlCl$_{1/1}$Cl$_{3/2}$ connectivity with the NaCl$_6$ unit interlinked by four AlCl$_4$ tetrahedra.

The structure of the hafnium-containing compound **3** is very similar to **2** and exhibits Hf–O distances of 201(3)–230(4)
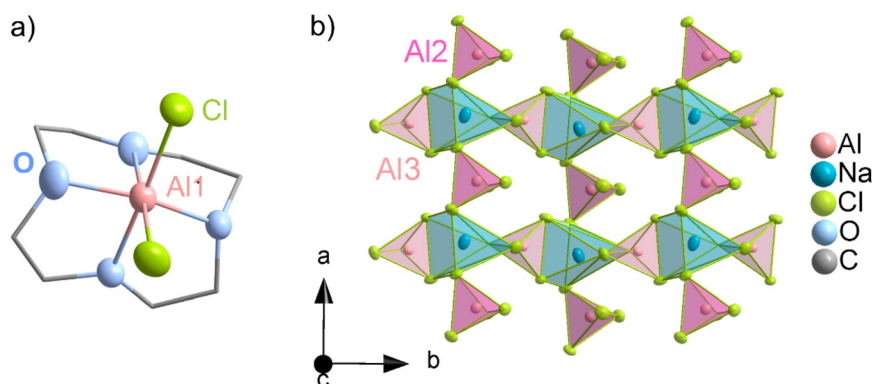

Fig. 3 Crystal structure of $[AlCl_2(12c4)][NaAl_2Cl_8]$ (**1**): (a) $[AlCl_2(12c4)]^+$ cation, (b) $^2_\infty[NaAl_2Cl_8]^-$ anion (hydrogen atoms not shown for clarity).
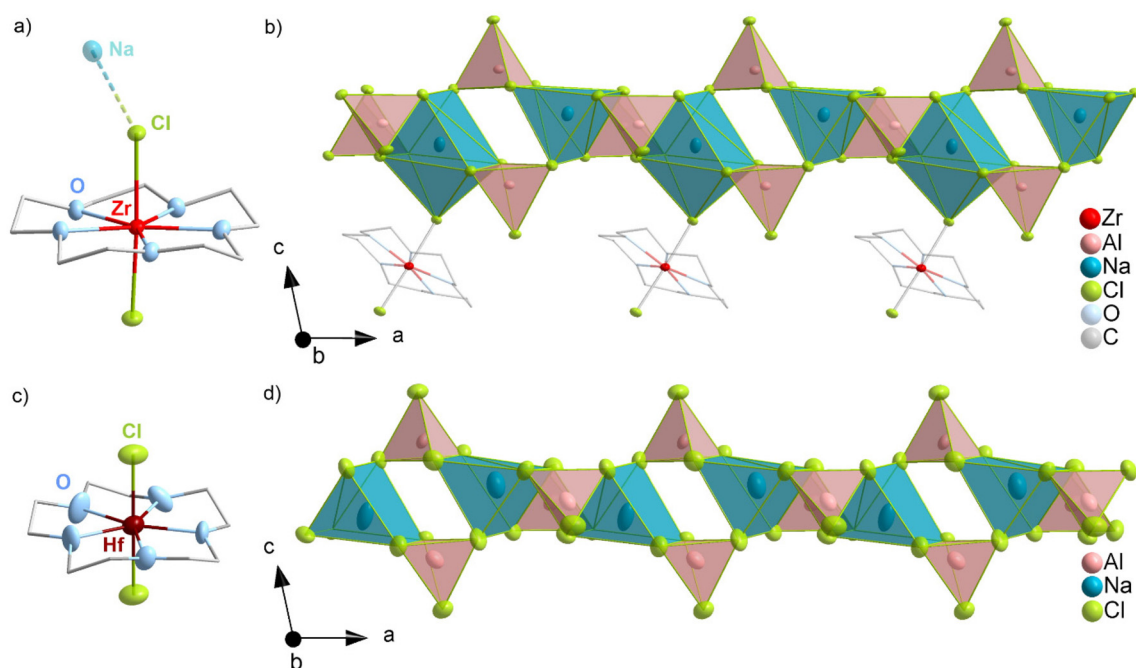
Fig. 4 Crystal structure of [MCl$_2$(15c5)][Na$_2$Al$_4$Cl$_{16}$] (with M: Zr (**2**) and Hf (**3**)): (a) [ZrCl$_2$(15c5)]$^+$ cation, (b) $\frac{1}{\infty}$[Na$_2$Al$_4$Cl$_{16}$]$^-$ anion, (c) [HfCl$_2$(15c5)]$^+$ cation, (d) $\frac{1}{\infty}$[Na$_2$Al$_4$Cl$_{16}$]$^-$ anion (hydrogen atoms and disorder not shown for clarity; data collection for **2** at 100 K on Stoe Stadivari diffractometer; data collection for **3** at 293 K on Stoe IPDS2 diffractometer; see ESI†).

pm for the [HfCl$_2$(15c5)]$^{2+}$ cation (Fig. 4c). In contrast to [ZrCl$_2$(15c5)]$^{2+}$, [HfCl$_2$(15c5)]$^{2+}$ interestingly shows positional disorder of 15c5, which was tackled by occupancies of 62 and 38%. Moreover, it needs to be noticed that the distance between the [HfCl$_2$(15c5)]$^{2+}$ cation and the $\frac{1}{\infty}$[Na$_2$Al$_4$Cl$_{16}$]$^{2-}$ chain is elongated in **3** (Na–Cl: 349.9(20) pm), so that – in contrast to **2** – the NaCl$_6$ prism of Na(2) is not capped.

In addition to the reaction of Zr(0) and Hf(0) nanoparticles with 15c5 in [BMIm]Cl/AlCl$_3$, both metal nanoparticles were also reacted with 18c6 in [BMIm]Cl/AlCl$_3$. Interestingly, the compounds **2** and **3** were formed again in large quantities. This requires a ring opening of 18c6 with a size reduction to 15c5, which, in fact, was similarly reported in the literature for other reactions.[4,19] Finally, it can be concluded that a coordination of Zr^{4+}/Hf^{4+} with 15c5 is obviously preferred over a coordination with the smaller 12c4 or the larger 18c6.

To verify the unexpected fragmentation of 18c6 in the reaction with the Zr(0) nanoparticles, we have performed a similar reaction of 18c6 with Sc(0) nanoparticles as Sc^{3+} (r(Sc^{3+}) = 75 pm)[17] is of similar size as Zr^{4+} (r(Zr^{4+}) = 73 pm),[17] however, with a lower charge and, therefore, also reduced Lewis acidity. The reaction of Sc(0) nanoparticles and 18c6 in [BMIm]Cl/AlCl$_3$ at 120 °C resulted in colourless plates of [ScCl$_2$(18c6)][AlCl$_4$] (**4**) according to the reaction:

$$\text{Sc} + 18\text{c6} + 2\text{AlCl}_3 \rightarrow [\text{ScCl}_2(18\text{c6})][\text{AlCl}_4] + \text{Al}.$$
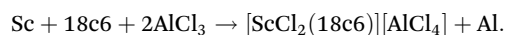
The reactivity of all metal nanoparticles is obviously high enough to reduce Al^{3+} from the ionic liquid to Al(0). The presence of aluminum was also confirmed by a greyish solid

formed during the reaction and similarly observed in previous reactions.[9a] **4** crystallizes in the non-inversion symmetric space group *Pna*2$_1$ (ESI: Table S4 and Fig. S4†) and contains [ScCl$_2$(18c6)]$^+$ cations and [AlCl$_4$]$^-$ anions (Fig. 5). Indeed, 18c6 was not split during the reaction but binds only with 5-of-6 oxygen atoms to Sc^{3+} (Sc–O: 219.7(6)–223.9(6) pm) (Fig. 5a). This observation again points to the fact that 15c5 and a coordination with 5 oxygen atoms is most preferable for a high-charged cation, about 75 pm in size. In addition to 18c6, Sc^{3+} is axially coordinated by two Cl$^-$ (Sc–Cl: 241.6(2), 244.2(2) pm), resulting in a distorted pentagonal bipyramidal coordination (O$_{eq}$–Sc–O$_{eq}$: 69.0(2)–77.9(2)°; Cl$_{ax}$–Sc–Cl$_{ax}$: 176.9(1)–178.1(1)°). Certain distortion results from the non-coordinating oxygen atom of 18c6, which, for instance, leads to a deviation of the Cl–Sc–Cl angle from the ideal 180° angle. Finally, it needs to be noticed that the non-coordinated oxygen atom shows positional disorder, which was tackled by split positions with occupancies of 83 and 17%. The [ScCl$_2$(18c6)]$^+$ cation is already known from [ScCl$_2$(18c6)][FeCl$_4$] and [ScCl$_2$(18c6)][SbCl$_6$] showing similar distances (Sc–O: 219–226 pm; Sc–Cl: 240–244 pm).[20]

In addition to single-crystal structure analysis, the compounds **1–4** were examined by vibrational spectroscopy (ESI: Fig. S5–S7†). As crystals of the title compounds can hardly be separated from the ionic liquid, vibrations of the [BMIm]$^+$ cation are observed in addition to the vibrations of the crown ether in Fourier-transform infrared (FT-IR) spectra. Thus, ν(C–H) vibrations at 3000–2800 cm^{-1} originate from both the [BMIm]$^+$ cation and the respective crown ether. Furthermore,

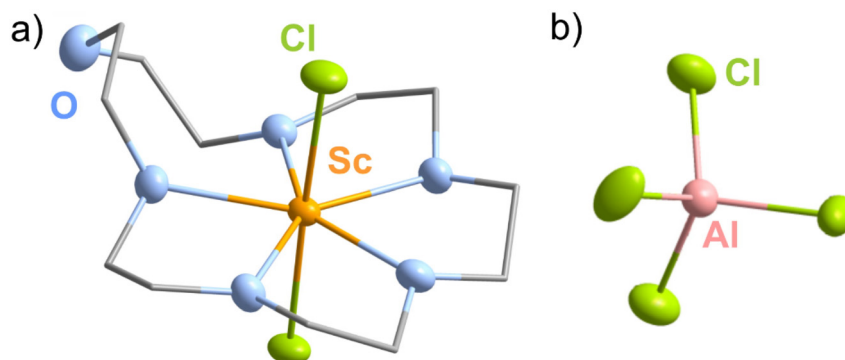**Fig. 5** Crystal structure of [ScCl$_2$(18c6)][AlCl$_4$] (**4**): (a) [ScCl$_2$(18c6)]$^+$ cation, (b) [AlCl$_4$]$^−$ anion (hydrogen atoms and disorder not shown for clarity).

ν(C=N) (1650–1600 cm^{-1}) stems from [BMIm]$^+$. The ν(C–O) vibrations at 1150–1000 cm^{-1} indicate the presence of the crown ether, whereas the fingerprint range (1000–500 cm^{-1}) again relates to ν(C–C), δ(C–C), δ(C–H) vibrations of the [BMIm]$^+$ cation and of the respective crown ether. A certain shift to higher wavenumbers in comparison to the pure crown ether, furthermore, can be attributed to the coordination of the crown ether to a cation in **1–4**. At low wavenumbers, the intense absorption at 480–465 cm^{-1} is characteristic for ν(Al–Cl) of the AlCl$_4^-$ tetrahedra. Finally, the absence of any O–H related vibrations at 3500–3300 cm^{-1} evidences the absence of moisture.

3.3 Nonlinear optical properties

As the compounds **1–4** crystallize in space groups without inversion symmetry, non-linear optical (NLO) effects are to be expected. In fact, the compounds **2** and **4** appear to be interesting for NLO effects due to the ordered arrangement of their building units in the space groups $P2_1$ and $Pna2_1$.[11] In order to validate potential NLO effects and to verify their performance, second harmonic generation (SHG) was studied for **2** and **4** based on the Kurtz-Perry approach.[21] Specifically for new compounds, the Kurtz-Perry approach offers several advantages. First of all, SHG measurements can be performed with microcrystalline powder samples. Moreover, the presence of enantiomeric or twinned crystals is not an issue if the individual domains are larger than 1 μm. The Kurtz-Perry approach also allows to distinguish between matchable and non-phase matchable materials due to the relationship between the SHG intensities and the grain sizes. However, the Kurtz-Perry approach also has limitations. Thus, only averaged effective SHG coefficients are provided with large uncertainty as it is difficult to quantify the grain-size distribution in a powder sample.

For the compounds **2** and **4**, unsorted powder samples with non-defined grain sizes were exposed to laser light with a wavelength of 1064 nm. The converted light was detected at 532 nm. The measured SHG intensities are shown in Tables 2 and 3. As the crystals are colourless, they are transparent in the spectral regime of the incident laser as well as in the spectral regime of the converted light. As the Kurtz-Perry approach

Table 2 SHG intensity of [ZrCl$_2$(15c5)][Na$_2$Al$_4$Cl$_{16}$] (**2**) in comparison to reference samples. All measurements were performed with the Kurtz-Perry approach[21]

Sample	Particle size (μm)	SHG intensity (mV)
Quartz	<5	29(10)
Quartz	5–25	238(28)
Quartz	25–50	380(81)
Al$_2$O$_3$	9	0(1)
KDP	5–25	730(38)
KDP	25–50	1932(367)
[ZrCl$_2$(15c5)][Na$_2$Al$_4$Cl$_{16}$] (**2**)	Non-defined	1(1)

Table 3 SHG intensity of [ScCl$_2$(18c6)][AlCl$_4$] (**4**) in comparison to reference samples. All measurements were performed with the Kurtz-Perry approach[21]

Sample	Particle size (μm)	SHG intensity (mV)
Quartz	<5	34(8)
Quartz	5–25	105(18)
Quartz	25–50	197(62)
Al$_2$O$_3$	9	0(1)
KDP	5–25	448(57)
KDP	25–50	1787(661)
[ScCl$_2$(18c6)][AlCl$_4$] (**4**)	Non-defined	1118(123)

does not result in absolute SHG intensities, quartz and potassium dihydrogenphosphate (KH$_2$PO$_4$, KDP) were examined as references with similar conditions to compare the intensity of the SHG signals. KDP is phase matchable (second-order susceptibility: d_{36} = 0.39 pm V^{-1}), and therefore yields a SHG signal at least 5-times stronger than for the non-phase-matchable quartz (d_{11} = 0.3 pm V^{-1}) although the SHG coefficients of KDP and quartz are similar.[22] Furthermore, corundum (α-Al$_2$O$_3$) was analyzed as a reference with a center of inversion, which does not show any SHG effect. In comparison to the references, **4** shows strong SHG signals, comparable to KDP (Table 3). The SHG-intensity of compound **2** is comparable to the centrosymmetric reference (Table 2). However, it must be taken into account that grain size, grain-size distribution, and layer thickness are yet non-defined for the new compounds **2** and **4**.

In addition to the experimental determination of the SHG intensities, the SHG tensors for **2** and **4** were computed using density functional theory (DFT) calculations assuming Kleinmann symmetry. The complete tensors are listed in Tables 4 and 5. We computed average effective SHG coefficients (d_{eff}) to facilitate a comparison. The d_{eff} value of **4** is 0.22 pm V^{-1}, while the d_{eff} value of **2** is 0.04 pm V^{-1}. The corresponding values for quartz are d_{eff}(quartz) = 0.21 pm V^{-1}, while for KDP d_{eff}(KDP) is 0.33 pm V^{-1}. The representation surfaces of the SHG tensor of **4** were calculated and displayed as two-dimensional projections (ESI: Fig. S8†) and three-dimensional projection (Fig. 6). Within the substantial uncertainties of both computation and experiment, these values are consist-

ent with the ratio of the observed SHG intensity of **4** to that of KDP, and indicate a 6–10-times larger SHG intensity compared to the non-phase matchable quartz. This also implies that **4** is phase-matchable. Additional measurements of the grain-size dependence of SHG signals could provide further experimental constraints for the phase-matching conditions, but these were outside the scope of the present study. In the case of compound **2**, the results of both the experiment and the theory indicate a very weak SHG effect close to zero. The reason for this could be the arrangement of the structural groups, which are nearly centrosymmetric with an approximate inversion and resulting in some very weak net polarization. Based on the SHG experiment, this possibly implies a close to centrosymmetric structural model of the heavier atoms for compound **2**.

Table 4 Calculated SHG tensor coefficients of [ZrCl$_2$(15c5)][Na$_2$Al$_4$Cl$_{16}$] (**2**) (pm V^{-1})

	d_{x1}	d_{x2}	d_{x3}	d_{x4}	d_{x5}	d_{x6}
d_{1y}	0.00	0.00	0.00	0.03	0.00	−0.03
d_{2y}	−0.03	−0.04	−0.03	0.00	0.03	0.00
d_{3y}	0.00	0.00	0.00	−0.03	0.00	0.03

Table 5 Calculated SHG tensor coefficients of [ScCl$_2$(18c6)][AlCl$_4$] (**4**) (pm V^{-1})

	d_{x1}	d_{x2}	d_{x3}	d_{x4}	d_{x5}	d_{x6}
d_{1y}	0.00	0.00	0.00	0.00	−0.16	0.00
d_{2y}	0.00	0.00	0.00	−0.27	0.00	0.00
d_{3y}	−0.16	−0.27	0.27	0.00	0.00	0.00

4. Conclusions

The base metals zirconium, hafnium and scandium are realized *via* liquid-phase syntheses by reduction of ZrCl$_4$, HfCl$_4$ and ScCl$_3$ with sodium naphthalenide in THF at room temperature. The as-prepared Zr(0), Hf(0), Sc(0) nanoparticles are monocrystalline and exhibit a particle diameter of 2–8 nm with narrow size distribution (Zr(0): 4.0 ± 0.9 nm; Hf(0): 8.0 ± 3.9 nm; Sc(0): 2.4 ± 0.2 nm). These metal nanoparticles are highly reactive (*e.g.* as powder samples when in contact to air) and can react with spontaneous ignition. Under inert conditions, the Zr(0), Hf(0), Sc(0) nanoparticle suspension in THF or toluene are chemically and colloidally very stable and offer the option for a use as starting materials in the liquid phase. Due to the small size of the nanoparticles, reactions are performed at the border of heterogeneous and homogenous conditions, allowing syntheses that would hardly be possible with the respective bulk metals.

Exemplarily, the as-prepared Zr(0), Hf(0), Sc(0) nanoparticles are reacted with the crown ethers 12-crown-4 (12c4), 15-crown-5 (15c5) and 18-crown-6 (18c6). Reactions were performed in ionic liquids that, on the one hand, are weakly coordinating and, on the other hand, chemically highly stable. The crown ethers were selected since knowledge on crown-ether coordination compounds of zirconium, hafnium and scandium is generally limited until now. Moreover, the selected crown ethers offer different ring-opening diameters of 140 to 300 pm, which may allow different coordinative situations. As a result, the four new crown-ether coordination complexes [AlCl$_2$(12c4)][NaAl$_2$Cl$_8$] (**1**), [ZrCl$_2$(15c5)][Na$_2$Al$_4$Cl$_{16}$] (**2**), [HfCl$_2$(15c5)][Na$_2$Al$_4$Cl$_{16}$] (**3**), and [ScCl$_2$(18c6)][AlCl$_4$] (**4**) were obtained. They show interesting structural features, including layered structures (**1**), chiral chain-type compounds (**2,3**) and isolated ions (**4**). All compounds crystallize in space groups without inversion symmetry. Second-harmonic generation (SHG) was evidenced for [ZrCl$_2$(15c5)][Na$_2$Al$_4$Cl$_{16}$] (**2**) and [ScCl$_2$(18c6)][AlCl$_4$] (**4**). While **2** shows a moderate SHG effect, specifically **4** exhibits a strong SHG signal comparable to KH$_2$PO$_4$/KDP and implies to be phase matchable.
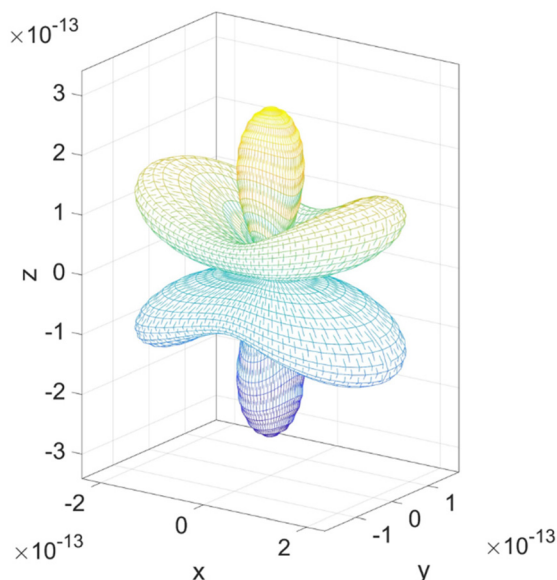

Fig. 6 Three-dimensional projection of the representation surfaces of tensor $d'_{333} = \alpha_{3i}\alpha_{3j}\alpha_{3k}d_{ijk}$ for [ScCl$_2$(18c6)][AlCl$_4$] (**4**) (for two-dimensional projections of the representation surfaces see ESI: Fig. S8†). The α_{3i}, α_{3j} and α_{3k} are direction cosines.

Besides the novel base-metal nanoparticles and the novel crown-ether coordination compounds, the applied redox approach of using suspended reactive metal nanoparticles could generally be an interesting option for chemical synthesis and the preparation of new compounds with interesting properties.

Data availability

Additional data regarding experiments and methods can be obtained from the ESI† and on request from the authors.

Conflicts of interest

The authors declare no competing financial interest.

Acknowledgements

References

1 (a) J. S. Bradshaw, R. M. A. Izatt, V. Bordunov, C. Y. Zhu and J. K. Hathaway, in *Crown ethers*, ed. G. W. Gokel, *Comprehensive Supramolecular Chemistry*, 1996, vol. 1, p. 35; (b) Z. Liu, S. K. M. Nalluri and J. F. Stoddart, *Chem. Soc. Rev.*, 2017, **46**, 2459–2478.

2 (a) M. S. Fonari, N. G. Furmanova and Yu. A. Simonov, *J. Struct. Chem.*, 2009, **50**, S124–S135; (b) A. B. Ilyukhin and S. P. Petrosyants, *Russ. J. Coord. Chem.*, 2007, **33**, 265–271; (c) H. R. Webb, M. J. Hardie and C. L. Raston, *Chem. – Eur. J.*, 2001, **7**, 3616–3620.

3 (a) R. F. Munha, M. A. Antunes, L. G. Alves, L. F. Veiros, M. D. Fryzuk and A. M. Martins, *Organometallics*, 2010, **29**, 3753–3764; (b) E. A. Babaian, D. C. Hrncir, S. G. Bott and J. L. Atwood, *Inorg. Chem.*, 1986, **25**, 4818–4821.

4 (a) A. Alvanipour, J. L. Atwood, S. G. Bott, P. C. Junk, U. H. Kynast and H. Prinz, *J. Chem. Soc., Dalton Trans.*, 1998, **7**, 1223–1228; (b) H. Prinz, S. G. Bott and J. L. Atwood, *J. Am. Chem. Soc.*, 1986, **108**, 2113–2114.

5 (a) M. D. Brown, W. Levason, D. C. Murray, M. C. Popham, G. Reid and M. Webster, *Dalton Trans.*, 2003, **5**, 857–865; (b) G. R. Willey, P. R. Meehan, M. D. Rudd and G. B. Drew, *J. Chem. Soc., Dalton Trans.*, 1995, **5**, 811–817; (c) G. R. Willey, M. T. Lakin and N. W. Alcock, *J. Chem. Soc., Dalton Trans.*, 1993, **22**, 3407–3411.

6 N. Wiberg, E. Wiberg and A. F. Holleman, *Anorganische Chemie*, de Gruyter, Berlin, 103rd edn, 2017, vol. 2, p. 1809.

7 G. B. Sergeev and K. J. Klabunde, *Nanochemistry*, Elsevier, Amsterdam, 2nd edn, 2013, pp. 157–175.

8 (a) I. Michelakaki, N. Boukos, D. A. Dragatogiannis, S. Stathopoulos, C. A. Charitidis and D. Tsoukalas, *Beilstein J. Nanotechnol.*, 2018, **9**, 1868–1880; (b) M. Eshed, S. Pol, A. Gedanken and M. Balasubramanian, *Beilstein J. Nanotechnol.*, 2011, **2**, 198–203; (c) M. Tokushige, T. Nishikiori and Y. Ito, *Russ. J. Electrochem.*, 2010, **46**, 619–626.

9 (a) L.-P. Faden, A. Reiß, R. Popescu, C. Donsbach, J. Göttlicher, T. Vitova, D. Gerthsen and C. Feldmann, *Inorg. Chem.*, 2024, **63**, 1020–1034; (b) D. Bartenbach, O. Wenzel, R. Popescu, L.-P. Faden, A. Reiß, M. Kaiser, A. Zimina, J.-D. Grunwaldt, D. Gerthsen and C. Feldmann, *Angew. Chem., Int. Ed.*, 2021, **60**, 17373–17377.

10 V. K. LaMer and R. H. J. Dinegar, *J. Am. Chem. Soc.*, 1950, **72**, 4847–4854.

11 A. W. Hull, *Phys. Rev.*, 1921, **18**, 88–89.

12 P. A. Romans, O. G. Paasche and H. Kato, *J. Less-Common Met.*, 1965, **8**, 213–215.

13 B. Hajek, V. Brozek and P. H. Duvigneaud, *J. Less-Common Met.*, 1973, **33**, 385–386.

14 L. Fabbrizzi, *Cryptands and Cryptates*, World Scientific, New Jersey, 2018.

15 P. Wasserscheid and T. Welton, *Ionic Liquids in Synthesis*, Wiley-VCH, Weinheim, 2008.

16 M. M. Olmstead and P. P. Power, *J. Am. Chem. Soc.*, 1986, **108**, 4235–4236.

17 R. D. Shannon, *Acta Crystallogr., Sect. A*, 1976, **32**, 751–767.

18 H. Elgamal, G. Robinson, S. Bott, J. Weeks, W. Hunter and J. Atwood, *J. Inclusion Phenom.*, 1984, **2**, 367–376.

19 H. Prinz, S. G. Bott and J. L. Atwood, *J. Am. Chem. Soc.*, 1986, **108**, 2114–2116.

20 (a) M. D. Brown, W. Levason, D. C. Murray, M. C. Popham, G. Reid and M. Webster, *Dalton Trans.*, 2003, **3**, 857–865; (b) G. R. Willey, M. T. Lakin and N. W. Alcock, *J. Chem. Soc., Chem. Commun.*, 1992, 1619–1620.

21 S. K. Kurtz and T. T. Perry, *J. Appl. Phys.*, 1968, **39**, 3789–3818.

22 L. Garvie, P. Rez, J. Alvarez, P. Buseck, A. Craven and R. Brydson, *Am. Mineral.*, 2000, **85**, 732–738.